

Separation of Transparent Layers by Polarization Analysis*

Yoav Y. Schechner Nahum Kiryati[†] Joseph Shamir

Department of Electrical Engineering,
Technion - Israel Institute of Technology,
Haifa, Israel 32000

`yoavs@tx.technion.ac.il`
`jsh@ee.technion.ac.il`

[†]Department of Electrical Engineering-Systems,
Faculty of Engineering, Tel-Aviv University,
Ramat Aviv, Israel 69978

`nk@eng.tau.ac.il`

Abstract

Consider the phenomenon of a virtual image, semi-reflected by a transparent medium (e.g. a glass window) present in the scene. The semi-reflected image is superimposed on the image of the object that is behind the transparent medium. A novel approach is proposed for the recovery of the superimposed layers. An initial separation of the layers is obtained using the raw output of a polarizing filter placed in front of the camera at two polarizer orientations. This separation is insufficient at most incidence angles. However, each pixel value in the two raw images is a linear combination of the corresponding pixel values in the separate layers. The corresponding weights depend on the reflection coefficients of each polarization component. The reflection coefficients are modified to account for changes in the reflection and polarizing properties due to internal reflections within the medium. In principle, the separate layers are obtained by pixel-wise inversion of the image formation process. Experimental results, obtained using real photos of actual objects, demonstrate the great superiority of the suggested method over using only raw optical data.

Keywords: Transparent layers, Reflection, Polarization imaging, Physics based vision.

1 Introduction

In the computer vision and image processing fields, it has usually been assumed that the depth and intensity,

at each point of the image, are single valued. However, the situation in which several (typically two) linearly superimposed contributions exist is often encountered in real-world scenes. For example [5, 6, 11, 15], looking out of a car (or room) window, we see both the outside world (termed *real object* [9, 10, 11]), and a semi-reflection of the objects inside, termed *virtual objects* (Fig. 1).

The treatment of such cases is important, since the combination of several unrelated images is likely to degrade the ability to analyze and understand them. In particular, the phenomenon may cause ambiguities that will confuse vision algorithms based on feature matching (such as motion and stereo). As the real and virtual objects will usually be at different distances from the camera, this situation can certainly confuse autofocus devices. The detection of the phenomenon is of importance itself, since it indicates the presence of a clear, transparent surface in front of the camera, at a distance closer than the imaged objects [9, 11] that contribute to the superposition.

The term *transparent layers* has been used to describe situations in which a scene is semi-reflected from a transparent surface [5, 2]. The image is decomposed into depth ordered layers, each with an associated map describing its intensity (and, if applicable, its depth or motion). We adopt this terminology, but stress the fact that we do not deal with imaging through an object with variable opacity (although this is the common usage of the term *transparency*). Approaches to reconstructing each of the layers by nulling the other relied mainly on motion [5, 2, 7, 12], stereo [14], and focus [11]. Although algorithms were developed to cope with this problem, fundamental ambiguities in the solutions were discovered [13, 17]. Moreover, methods for the separation of superimposed scenes that rely on defocus-blur, stereo

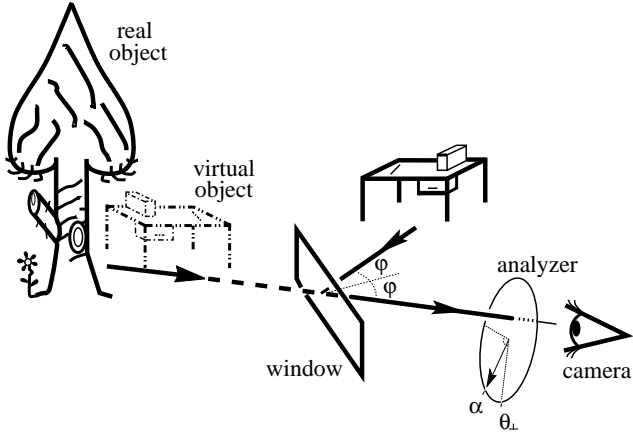


Figure 1: The image of a real object is partly transmitted via a transparent window which partly reflects the image of another object at angle φ , creating a virtual image of it. The combined scene can be viewed through a polarization analyzer (filter) at angle α . The plane of incidence includes the incident ray and the normal to the window. The best transmission of the polarization component perpendicular to this plane is when the analyzer is oriented at some value of α denoted θ_{\perp} .

or motion, are ill conditioned in the reconstruction of the low-frequency components, and the DC reconstruction is ill posed [11]. They also rely on the assumption that the superimposing layers lie at significantly different optical distances from the camera [11], thus having different stereo disparities, or different focused states of the imaging system, or different motion fields. Another major disadvantage of these methods is that they cannot determine which of the reconstructed images is of the real object and which is of the virtual one.

An approach based on polarimetry can avoid these problems, as it basically does not rely on spatial calculations. Polarimetric imaging has drawn interest [4, 8, 16, 19, 20, 21, 22] in recent years. Cameras that enable fast and reliable polarization imaging were constructed [4, 6, 19, 20, 21, 22] and used in various applications. One application is the removal of specular reflections superimposed on diffuse scattering from opaque surfaces [8, 18].

Polarization may be applied to the problem of separating and reconstructing transparent layers, since the virtual layer is specularly reflected from the transparent surface. Suppressing the contribution of semi-reflected layers by incorporating a polarizer into the imaging system is a well known photographic technique [15]. Some previous works attempted to remove the virtual layer by using just the raw output of the polarization analyzer (Fig. 1) in front of the camera [6, 9]. These methods suggested taking several images of the scene at different states of the polarizer, and picking one of them as the

reconstruction of the real layer. However, optical filtering eliminates the reflected (virtual) layer only at a specific incidence angle, called the *Brewster angle* [1, 3, 15], which is about 56° for glass (good filtering was demonstrated in [9] at this angle). Away from the Brewster angle, the optical filtering may improve the visibility of the real object, but cannot eliminate the increasing crosstalk with the virtual layer.

In this work we suggest and demonstrate a novel method for the separation of transparent (semi-reflected) layers. Initial separation is obtained using the raw output of a polarization analyzer (filter) in front of the camera. Then, weighted differences between the acquired images yield reconstructions of the images of the real object and the virtual object. The weights in these differences are derived directly from a physical analysis of the reflectance and transmission processes.

In the analysis of the physical processes, we take into account the effects of internal (secondary) reflections within two-surfaced reflecting media, such as glass windows. We show that these effects are significant both in terms of the reflection coefficients and in terms of the polarizing effects of the reflection and transmission processes. We show that contrary to common belief, the polarization of the transmitted scene may be dominant, rather than the polarization of the reflected one, even in moderate angles of incidence.

After calculating the appropriate reflection coefficients, we formulate the image formation process, i.e., the combination of two image sources, each with two polarization components, when viewed through a polarization analyzer. The basic reconstruction approach is the inversion of this process (when invertible), using two raw images acquired through the polarization analyzer. Since the approach is based on differences between images, it is sensitive to slight misalignments that occur when the analyzer is mechanically rotated as part of the acquisition procedure. We suggest an algorithm that greatly reduces the damaging effects of this phenomenon.

The approach presented here for the separation and reconstruction of transparent layers has several advantages with respect to previous approaches. Unlike methods that rely on stereo, motion and defocus blur, the proposed method does not suffer from ill-conditioning at the low frequencies, can easily resolve the DC component, and classifies which of the layers is the reflected (virtual) one and which is the real (transmitted) one. It does not require the layers to have different depths or motion fields. In addition, it allows operation away from the Brewster angle and gives far better results than those that can be achieved by using only raw optical data.

2 Internal reflections

In this section we derive the intensity transmission and reflection coefficients of a double-surfaced transparent medium, such as a glass window. The ray incident on a surface (like the front face of window) is partly reflected from the surface, and partly transmitted through it. All rays are in the same plane (Fig. 2), termed *the plane of incidence* [1, 3, 19]. We divide the intensity to two components¹: I_{\parallel} , for which the polarization is *parallel* to the plane of incidence, and I_{\perp} , for which the polarization is *perpendicular* to it. Each component has, respectively, reflection and transmission coefficients, R_{\parallel}, R_{\perp} and T_{\parallel}, T_{\perp} .

For a single-surface medium (e.g., water in a lake), the reflection coefficients are [1, 3]

$$R_{\parallel} = \frac{\tan^2(\varphi - \varphi')}{\tan^2(\varphi + \varphi')} , \quad R_{\perp} = \frac{\sin^2(\varphi - \varphi')}{\sin^2(\varphi + \varphi')} , \quad (1)$$

where φ is the angle of incidence (see Fig. 2). φ' is the angle of the refracted ray, which is related by Snell's law $n \sin \varphi' = \sin \varphi$, where n is the refractive index of the reflecting medium (≈ 1.5 for glass). From energy conservation considerations,

$$T_{\parallel} = 1 - R_{\parallel} , \quad T_{\perp} = 1 - R_{\perp} , \quad (2)$$

in case no absorption occurs in the surface. The same coefficients are obtained for a ray passing from the dense medium (e.g. glass) to the air.

Cases of reflection from double-surfaced media are, however, by far more common than reflection by a single surface. Typical examples are glass or polycarbonate windows and covers of pictures. As the light ray within the window is refracted to the air at the back surface (Fig. 2), part of it is reflected back to the front surface, from which refraction occurs again, and so on. As we will show, the effect of internal reflections is generally significant, both in terms of the reflection coefficients, and in terms of polarization. For each polarization component the total coefficient of reflection is

$$\tilde{R} = R + T^2 R \sum_{l=0}^{\infty} (R^2)^l . \quad (3)$$

This is true if the absorption within the window is negligible, and if the spacing between the significant reflection orders is small relative to the variations in the image. The latter condition is usually satisfied since, due to the typically small value of R , only the first two orders are significant and since most parts of a typical image are smooth. However, this condition may not hold near brightness edges not aligned parallel to the plane

¹Natural light is usually partially linearly polarized [4], and only rarely has a circular polarization component [16]. We thus neglect the effects of circular polarization.

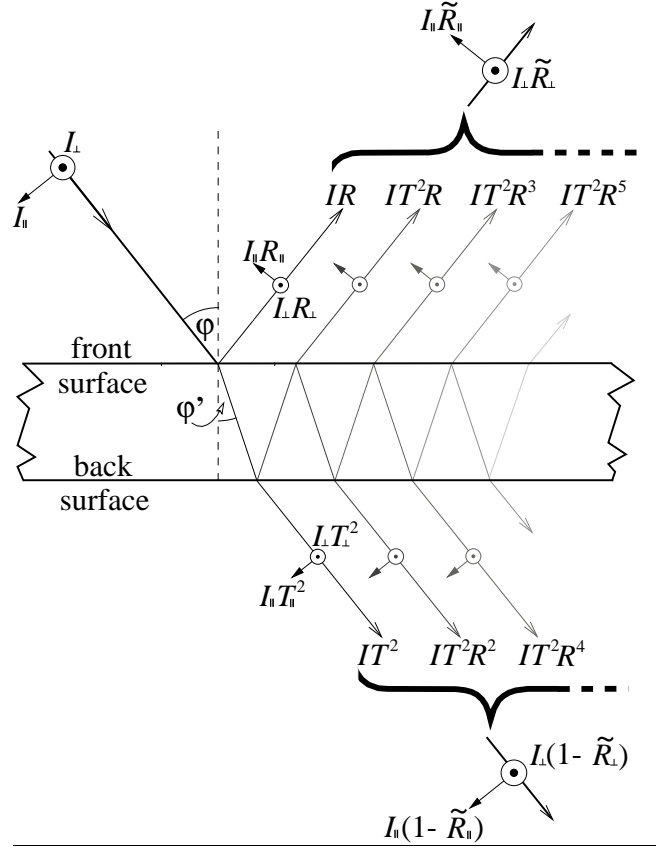


Figure 2: The plane of incidence. When a light ray is incident on any of the window surfaces, it undergoes reflection and refraction (transmission). The reflection (R) and transmission (T) coefficients for the component parallel (\parallel) to the plane of incidence are different than for the perpendicular (\perp) component. Internal reflections within the window give rise to orders of reflected/transmitted rays with decreasing intensities.

of incidence. Neglecting this effect (in this paper), we obtain that the total coefficients of reflection are

$$\tilde{R}_{\parallel} = \frac{2}{1 + R_{\parallel}} R_{\parallel} , \quad \tilde{R}_{\perp} = \frac{2}{1 + R_{\perp}} R_{\perp} , \quad (4)$$

and the transmission coefficients are

$$\tilde{T}_{\parallel} = \frac{1 - R_{\parallel}}{1 + R_{\parallel}} = 1 - \tilde{R}_{\parallel} , \quad \tilde{T}_{\perp} = \frac{1 - R_{\perp}}{1 + R_{\perp}} = 1 - \tilde{R}_{\perp} . \quad (5)$$

Note that the effect of internal reflections on the reflectivity is most significant when the reflection coefficient is small: if $R \ll 1$ the reflectivity of a double-surfaced medium (window) is *double* that of a single surface.

Consider now the influence of the window on the polarization. Since light is generally partially polarized, transmission through the analyzer (Fig. 1) is maximal for a certain analyzing angle α , and minimal for $\alpha + 90^\circ$. The intensities at these angles are denoted I_{\max} and

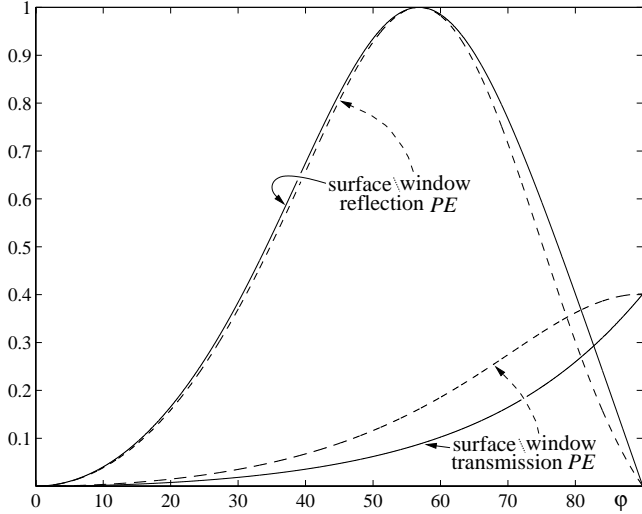


Figure 3: [Solid lines]: The polarizing effects (PE) of reflection and transmission through a single air-glass interface, as a function of the angle of incidence. [Dashed lines]: The polarizing effects of reflection and transmission through a glass window.

I_{\min} , respectively. The *degree of polarization* of partially polarized light is defined [8, 19, 21] as

$$\text{degree of polarization} = \frac{I_{\max} - I_{\min}}{I_{\max} + I_{\min}}. \quad (6)$$

We define the *polarizing effect* of a process, denoted $PE(\text{process})$, as the degree of polarization that it induces on unpolarized incident light. In the case of unpolarized light incident on a reflecting/transmitting surface, the highest transmission through the analyzer will be either if it is aligned parallel to the plane of incidence, or perpendicular to it. Thus the polarizing effects in a single-surface are

$$\begin{aligned} PE(\text{surface reflection}) &= \frac{|R_{\perp} - R_{\parallel}|}{|R_{\perp} + R_{\parallel}|} \\ PE(\text{surface transmission}) &= \frac{|T_{\perp} - T_{\parallel}|}{|T_{\perp} + T_{\parallel}|}. \end{aligned} \quad (7)$$

The polarizing effects of reflection and transmission through a single air-glass interface are plotted as solid lines in Fig. 3. Well known facts are manifested in this graph. The polarizing effect in reflection is full ($= 1$) for the Brewster angle [3], in which the parallel component vanishes. For most incidence angles the PE of reflection is larger than the PE of transmission. However, at high incidence angles the PE of transmission is larger than that of reflection.

The polarizing effects in a double-surface medium

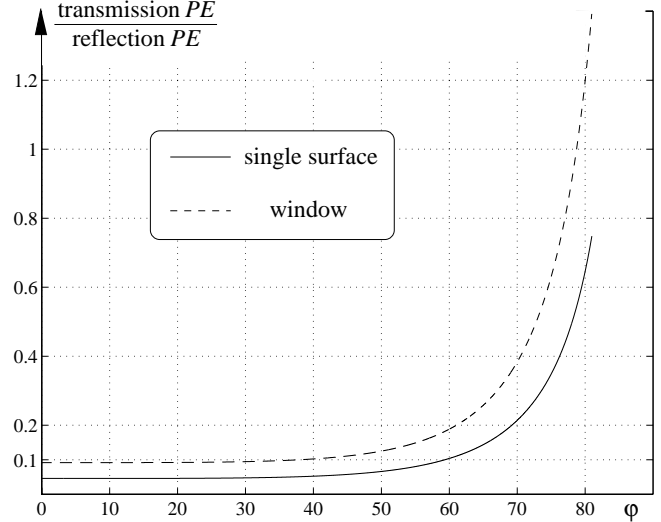


Figure 4: The relative polarizing effect of a single air-glass interface [solid line] and a glass window [dashed line], as a function of the angle of incidence.

(e.g., window) are

$$\begin{aligned} PE(\text{window reflection}) &= \frac{|\tilde{R}_{\perp} - \tilde{R}_{\parallel}|}{|\tilde{R}_{\perp} + \tilde{R}_{\parallel}|} \\ PE(\text{window transmission}) &= \frac{|\tilde{T}_{\perp} - \tilde{T}_{\parallel}|}{|\tilde{T}_{\perp} + \tilde{T}_{\parallel}|}. \end{aligned} \quad (8)$$

The polarization effects of reflection and transmission through a glass window are plotted as dashed lines in Fig. 3. The PE of reflection is somewhat smaller relative to the PE in a single surface. However, the PE of transmission is significantly larger and is almost twice as large at most incidence angles.

To better compare the polarizing effects, we define the *relative polarizing effect* as the ratio of the PE of transmission and that of reflection. As seen in Fig. 4, the polarizing effect of transmission through a window is about 10% (and even more) that of reflection for most incidence angles. Although it is small, it is not a negligible effect. We will show in Sec. 3, that it is common that the polarized component of the transmitted light is larger than that of the reflected one.

3 Image formation

We assume from this point on that the light emanated from the objects to be imaged is unpolarized (or with negligible polarization). Let I_T be the intensity (at a certain pixel) of the image of the real object without the window. Let I_R be the intensity (at the same pixel) of the image of the virtual object, had there been a perfect

mirror instead of the window. For an arbitrary cylindrical coordinate system, whose axis is parallel to the optical axis of the imaging system, we define θ_{\perp} as the orientation of the polarization analyzer for best transmission of the component perpendicular to the plane of incidence. Generally, the orientation of the analyzer (defined in the same coordinate system) is α . The contribution of the reflected scene is

$$f_R(\alpha) = \frac{I_R}{2} [\tilde{R}_{\perp} \cos^2(\alpha - \theta_{\perp}) + \tilde{R}_{\parallel} \sin^2(\alpha - \theta_{\perp})] , \quad (9)$$

while the contribution of the transmitted scene is

$$f_T(\alpha) = \frac{I_T}{2} [\tilde{T}_{\perp} \cos^2(\alpha - \theta_{\perp}) + \tilde{T}_{\parallel} \sin^2(\alpha - \theta_{\perp})] . \quad (10)$$

The total intensity is the sum of these contributions, $f(\alpha) = f_R(\alpha) + f_T(\alpha)$. At $\alpha = \theta_{\perp}$ and $\alpha = \theta_{\perp} + 90^\circ$ the intensities are

$$f_{\perp} = f(\theta_{\perp}) = (I_R \tilde{R}_{\perp} / 2 + I_T \tilde{T}_{\perp} / 2) \quad (11)$$

and

$$f_{\parallel} = f(\theta_{\perp} + 90^\circ) = (I_R \tilde{R}_{\parallel} / 2 + I_T \tilde{T}_{\parallel} / 2) \quad (12)$$

respectively. Hence,

$$f(\alpha) = \left(\frac{f_{\perp} + f_{\parallel}}{2} \right) + \left(\frac{f_{\perp} - f_{\parallel}}{2} \right) \cos[2(\alpha - \theta_{\perp})] . \quad (13)$$

Note that

$$f_{\perp} - f_{\parallel} = 0.5(\tilde{R}_{\perp} - \tilde{R}_{\parallel}) (I_R - I_T) . \quad (14)$$

Since $R_{\perp} \geq R_{\parallel}$ [1, 3], it can be shown that $\tilde{R}_{\perp} \geq \tilde{R}_{\parallel}$. The intensity of a semi-reflected scene (13) is therefore maximal at $\alpha = \theta_{\perp}$ if and only if $I_R > I_T$. If $I_T = I_R$ the light leaving the reflecting medium is unpolarized. If the real object is brighter than the virtual one, $I_T > I_R$, the intensity would be *minimal* at $\alpha = \theta_{\perp}$. This is in contrast to the fundamental idea in [9], which is based on the assumption that $f(\theta_{\perp}) = \max_{\alpha} f(\alpha)$. Cases for which $I_T > I_R$ are very common, for example, looking out of the room or the car window during daylight. Intuitively, the low *PE* of the transmission process (relative to reflection) at low and moderate incidence angles is compensated by the high transmission to reflection coefficients ratio at these angles. Thus the polarization of the transmitted light may be dominant, rather than the polarization of the reflected layer. Thus, one cannot assume that θ_{\perp} is associated with the highest output of the polarization analyzer when imaging semi-reflected (transparent) scenes.

4 Reconstruction

Suppose now that the geometry of the setup is known, that is, the plane of incidence (hence θ_{\perp}) and the angle of incidence φ are known, or can be estimated. We

believe that this is a common case. For example, when watching lakes or ponds the plane of incidence is vertical. When looking at shop windows, the plane of incidence is usually horizontal. Note that f_{\perp} and f_{\parallel} are not sensitive to small errors in the estimation of θ_{\perp} , since

$$\left. \frac{\partial f}{\partial \theta_{\perp}} \right|_{\alpha=\theta_{\perp}, \theta_{\perp}+90^\circ} = 0 . \quad (15)$$

The method detailed here is based on interaction with a human operator, that provides the required angles. In this case \tilde{R}_{\perp} and \tilde{R}_{\parallel} are known. Thus (11) and (12) are two linear equations with two unknowns, which together with Eq. (5) yield

$$I_T = \left(2 \frac{\tilde{R}_{\perp}}{\tilde{R}_{\perp} - \tilde{R}_{\parallel}} \right) f_{\parallel} - \left(2 \frac{\tilde{R}_{\parallel}}{\tilde{R}_{\perp} - \tilde{R}_{\parallel}} \right) f_{\perp} \quad (16)$$

and

$$I_R = \left(2 \frac{1 - \tilde{R}_{\parallel}}{\tilde{R}_{\perp} - \tilde{R}_{\parallel}} \right) f_{\perp} - \left(2 \frac{1 - \tilde{R}_{\perp}}{\tilde{R}_{\perp} - \tilde{R}_{\parallel}} \right) f_{\parallel} . \quad (17)$$

Eqs. (16,17) show that if the incidence is at the Brewster angle (for which $\tilde{R}_{\parallel} = 0$), I_T can be directly associated with f_{\parallel} , as demonstrated in [9]. But even at that angle, I_R is not proportional to $f_{\perp} - f_{\parallel}$ in contrast to [9]. Nevertheless, operation at Brewster's angle is a rare situation, and one should generally use Eqs. (16,17). Note that the reconstructions become unstable and noise sensitive as $(\tilde{R}_{\perp} - \tilde{R}_{\parallel}) \rightarrow 0$, that is, at low incidence angles. This is expected since the polarizing effects are very small (and even zero) at these angles, as seen in Fig. 3.

Eqs. (16,17) suggest that reconstruction may be done solely by pointwise calculations, comparing each pixel in f_{\perp} only with its corresponding pixel in f_{\parallel} . However, if the angle of the polarization analyzer is changed by mechanical rotation, problems that are no longer of pointwise nature may arise. It has been recognized [4, 8, 19, 20, 21] that mechanical rotation of the analyzer leads to small image distortions. This leads to the appearance of false edges in the reconstruction of a layer in locations where true edges exist in the other layer. A related phenomenon is the appearance of false polarization readings at image edges, in measurements that are based on the comparison of images taken at different analyzer angles [8, 19, 20, 21, 22].

The problem can be alleviated by using special hardware, namely liquid-crystal filters which are mechanically stationary [19, 20, 21, 22]. We suggest an image-processing approach to the problem, that attempts to cancel the effects of the false-edge generation mechanism. To understand that mechanism, recall that Eqs. (16,17) calculate differences between similar images. Suppose for the moment that the raw images are

identical. Local shifts in the raw images cause the difference image to have high gradients where the raw images have edges, while correctly aligned raw images do not lead to the appearance of false edges in the difference image.

Based on this observation, we attempt to align the images, such that locally the gradients in the resulting reconstructed (difference) image are minimized. It turns out that correction by global translation is inadequate, but small local translations lead to good results. Note that the presence of genuine edges is typically preserved by small local shifts.

In the method that we implemented, local shifts are limited to single pixel movements either horizontally or vertically. Extension of the algorithm to allow larger movements is straightforward. The algorithm for reconstructing I_R consists of the following steps:

1. For each pixel (x, y) select the orientation $o(x, y)$ (either “horizontal” or “vertical”) according to the local orientation of $\nabla(f_{\perp} + f_{\parallel})$. Create regions of coherent orientations by 2D-median (majority) filtering of $o(x, y)$ in a small neighborhood, yielding $\hat{o}(x, y)$.
2. For *Orientation* = vertical, horizontal :
 - (a) Let $f_{\perp,0} = f_{\perp}$. Let $f_{\perp,\mp 1}$ be f_{\perp} shifted by ∓ 1 pixel along *Orientation*.
 - (b) Calculate $I_{R,k}$ (where $k = -1, 0, 1$) by replacing f_{\perp} by $f_{\perp,k}$ in Eq. (17). For each of the three images, calculate the gradient image $\nabla I_{R,k}$.
 - (c) For each pixel (x, y) find the index $k(x, y)$ for which the gradient $\nabla I_{R,k}$ is smallest at that pixel.
 - (d) The map of $k(x, y)$ contains many random fluctuations. Create regions of coherent movement by 2D-median filtering of $k(x, y)$ in a small neighborhood, yielding $\hat{k}(x, y)$.
 - (e) For each pixel (x, y) , if $\hat{o}(x, y) = \textit{Orientation}$, the reconstructed value is

$$\hat{I}_R(x, y) = I_{R,\hat{k}(x,y)} \cdot$$

3. Next *Orientation*.

Estimation of I_T is similar. Note that no blurring operator is used throughout the processing.

5 Reconstruction experiment

5.1 Using optics alone

We imaged a scene composed of several objects through an upright glass window. The window semi-reflected another scene (virtual object). The combined scene is shown in (Fig. 5(a)). Note that all images in this section

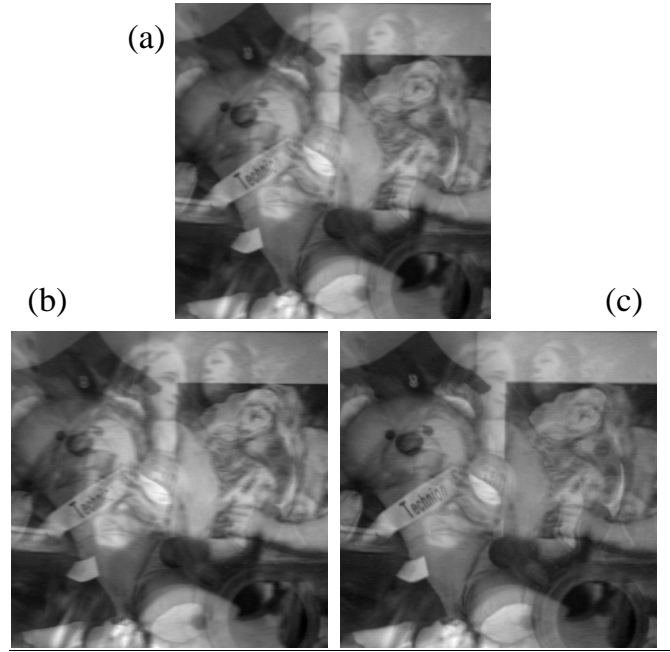


Figure 5: (a): The combined scene. (b): f_{\perp} . (c): f_{\parallel} . Although the reflected component is smaller in f_{\parallel} , the image is still unclear.

are contrast-stretched for clarity. The optical distance between the video camera and both scenes was about $\approx 3.5m$. A linear polarizer was rotated in front of the imaging system between consecutive image acquisitions. For good demonstration quality, 5 frames were averaged for each analyzer state. However, we should note that satisfying results were achieved also without averaging, i.e., acquiring a single frame for each state.

Since the plane of incidence is horizontal, we knew θ_{\perp} , thus we could take images of f_{\perp} and f_{\parallel} , shown² in Fig. 5. As can be seen in f_{\parallel} , the polarizer gives an initial attenuation of the reflected scene. Still, a significant disturbance due to the reflected scene remains, since the angle of incidence, 28° , was far from the Brewster angle. Thus optics alone does not solve the problem.

5.2 Using pointwise operations

We operated Eqs. (16,17) on each point in the images shown in Figs. 5(b,c). The results are shown in the top row of Fig. 6. The results can be compared with the separate “ground-truth” images shown in the bottom row of this figure. The reconstruction was very successful in most parts of the scenes. However, there still exists a disturbing crosstalk, especially seen in the reconstruction of the virtual object, in the form of traces of edges of the other layer, pointed out in Fig. 7.

²The raw images of f_{\perp} and f_{\parallel} are in an image database linked by <http://www.ee.technion.ac.il/~youavs/PUBLICATIONS/>



Figure 6: [Top row]: Reconstruction by pointwise operations. False edges are very disturbing in the virtual layer (as pointed out in Fig. 7). [Middle row]: Reconstruction using local shifting corrections. Most of the disturbing real-object edges disappeared from the reconstruction of the virtual object. [Bottom left]: The real object photographed without the interfering glass window. [Bottom right]: The virtual object photographed by removing the objects behind the glass window.

The interfering edges are not due to a fundamental problem in the physical model, in the assumptions or in the principles of reconstruction. Rather, this problem is technical. As noted above, it stems from distortions induced by the use of a mechanically-rotating analyzer. Indeed, when imaging the real object without the window (shown in the bottom-left of Fig. 6), false readings of polarization appeared at brightness edges, similar to those reported in [4, 8, 19, 20, 21, 22].



Figure 7: Reconstruction of the virtual layer by pointwise operations leaves significant traces of real-object edges (see arrows).

5.3 Using shift-corrections

We did not attempt to find a global transformation that models the distortion due to the mechanical rotation of the analyzer. Rather, we used the shifting-correction algorithm described in section 4. The results are shown in the middle row of Fig. 6. The improvement in the reconstruction of the virtual object is significant. Most of the disturbing false edges were removed, or largely attenuated. The reconstruction of the real object also shows weaker traces of the virtual object. Apparently, this operation did not cause any blurring of the true edges, and reconstructions are just as detailed as those obtained by pointwise operations.

Nevertheless, limiting the shift correction to 1 pixel (horizontally or vertically) is not always sufficient. Most notable is a horizontal false edge that appears near the top of the reconstructed virtual object. This is not caused by the lateral displacement of the secondary reflections, since the edge is parallel to the plane of incidence. We believe that a better shift-correction algorithm could solve this problem.

6 Discussion

Real and virtual objects superimposed by a reflecting surface can be well separated by image processing that follows polarimetric imaging. This is accomplished by using a proper reflection model (e.g., taking into account the effects of internal reflection within a glass window), and by the inversion of the physical equations of image formation. Using the proper reflectance coefficients al-

lows reconstruction away from the Brewster angle, that is, where the problem cannot be solved by optics alone. The method greatly extends the useful range of incidence angles, but is inapplicable if the angle of incidence is too small. Note that it is assumed that the light incident on the window is unpolarized. The consequences of partial polarization of the incident light are currently being studied.

The results presented in this work can be the basis for useful techniques in professional and amateur still-photography, where polarizers are commonly used. The method currently needs a human operator to feed it with the 3D orientation of the reflecting medium. We currently study ways to extract these parameters from the images themselves, leading to automatic operation.

Acknowledgment

This research was supported in part by the Israeli Ministry of Science.

References

- [1] R. M. A. Azzam and N. M. Bashara, *Ellipsometry and polarized light*, pp. 269-283 (North-Holland, Amsterdam, 1979).
- [2] J. R. Bergen, P. J. Burt, R. Hingorani and S. Peleg, "Transparent motion analysis" Proc. ECCV, pp. 566-569, 1990.
- [3] M. Born and E. Wolf, *Principles of optics*, 5th ed., pp. 38-45 (Pergamon, Oxford, 1975).
- [4] T. W. Cronin, N. Shashar and L. Wolff, "Portable imaging polarimeters," Proc. ICPR, Vol-A, pp. 606-609, 1994.
- [5] T. Darrell and E. Simoncelli, "Separation of transparent motion into layers using velocity-tuned mechanisms," TR-244, Media-Lab, MIT, 1993.
- [6] H. Fujikake, K. Takizawa, T. Aida, H. Kikuchi, T. Fujii and M. Kawakita, "Electrically-controllable liquid crystal polarizing filter for eliminating reflected light," Optical Review **5**, pp. 93-98, 1998.
- [7] M. Irani, B. Rousso and S. Peleg, "Computing occluding and transparent motions," Int. J. Comp. Vis. **12**, pp. 5-16, 1994.
- [8] S. K. Nayar, X. S. Fang and T. Boult, "Separation of reflection components using color and polarization," Int. J. Comp. Vis. **21**, pp. 163-186, 1997.
- [9] N. Ohnishi, K. Kumaki, T. Yamamura and T. Tanaka, "Separating real and virtual objects from their overlapping images," Proc. ECCV, Vol-II, pp. 636-646, 1996.
- [10] M. Oren and S. K. Nayar, "A theory of specular surface geometry," Proc. ICCV, pp. 740-747, 1995.
- [11] Y. Y. Schechner, N. Kiryati and R. Basri, "Separation of transparent layers using focus," Proc. ICCV, pp. 1061-1066, 1998.
- [12] M. Shizawa and K. Mase, "Simultaneous multiple optical flow estimation," Proc. ICPR pp. 274-278, 1990.
- [13] M. Shizawa, "On visual ambiguities due to transparency in motion and stereo," Proc. ECCV, pp. 411-419, 1992.
- [14] M. Shizawa, "Direct estimation of multiple disparities for transparent multiple surfaces in binocular stereo," Proc. ICCV, pp. 447-454, 1993.
- [15] W. A. Shurcliff and S. S. Ballard, *Polarized light* (Van Nostrand, Princeton, 1964).
- [16] R. Walraven, "Polarization imagery," Opt. Eng. **20**, pp. 14-18, 1981.
- [17] D. Weinshall, "Perception of multiple transparent planes in stereo vision," Nature **341**, pp. 737-739, 1989.
- [18] L. B. Wolff, "Using polarization to separate reflection components," Proc. CVPR, pp. 363-369, 1989.
- [19] L. B. Wolff, "Polarization camera for computer vision with a beam splitter," JOSA A **11**, pp. 2935-2945, 1994.
- [20] L. B. Wolff and A. Andreou, "Polarization camera sensors," Image and Vision Computing **13**, pp. 497-510, 1995.
- [21] L. B. Wolff, "Applications of polarization camera technology," IEEE Expert **10**, pp. 30-38, 1995.
- [22] L. B. Wolff, "Polarization vision: a new sensory approach to image understanding," Image and Vision Computing **15**, pp. 81-93, 1997.